remote sensing

MDPI

Article

Bathymetry Refinement over Seamount Regions from SAR Altimetric Gravity Data through a Kalman Fusion Method

Yihao Wu, Junjie Wang *, Yueqian Shen, Dongzhen Jia and Yu Li

School of Earth Sciences and Engineering, Hohai University, Nanjing 211100, China
* Correspondence: junjie2020@hhu.edu.cn

Abstract: Seafloor topography over seamount areas is crucial for studying plate motions, seafloor seismicity, and seamount ecosystems. However, seamount bathymetry modeling is difficult due to the complex hydrodynamic environment, biodiversity, and scarcity of shipborne echo sounding data. The use of satellite altimeter-derived gravity data is a complementary way of bathymetry computation; in particular, the incorporation of synthetic aperture radar (SAR) altimeter data may be useful for seamount bathymetry modeling. Moreover, the widely used filtering method may have difficulty in combing different bathymetry data sets and may affect the quality of the computed bathymetry. To mitigate this issue, we introduce a Kalman fusion method for weighting and combining gravity-derived bathymetry data and the reference bathymetry model. Numerical experiments in the seamount regions over the Molloy Ridge show that the use of SAR-based altimetric gravity data improves the local bathymetry model, by a magnitude of 14.27 m, compared to the result without SAR data. In addition, the developed Kalman fusion method outperforms the traditionally used filtering method, and the bathymetry computed from the Kalman fusion method is improved by a magnitude of 9.34 m. Further comparison shows that our solution has improved quality compared to a recently released global bathymetry model, namely, GEBCO 2022 (GEBCO: General Bathymetric Chart of the Oceans), by a magnitude of 34.34 m. The bathymetry model in this study may be substituted for existing global bathymetry models for geophysical investigations over the target area.

Keywords: seamount bathymetry refinement; altimetric gravity anomaly; synthetic aperture radar altimeter; Kalman fusion method

Citation: Wu, Y.; Wang, J.; Shen, Y.; Jia, D.; Li, Y. Bathymetry Refinement over Seamount Regions from SAR Altimetric Gravity Data through a Kalman Fusion Method. *Remote Sens.* **2023**, *15*, 1288. https://doi.org/10.3390/rs15051288

Academic Editors: Walyeldeen Godah, Xiaogong Hu and Mladen Zrinjski

Received: 4 January 2023
Revised: 22 February 2023
Accepted: 23 February 2023
Published: 26 February 2023

1. Introduction

Bathymetry information plays an important role in studying the biodiversity over seamount areas, monitoring seafloor faults caused by earthquakes, and investigating the effects of seamounts on ocean hydrodynamic environments [1–3]. The global bathymetry models—e.g., the recently released global model, namely GEBCO_2022 (GEBCO: General Bathymetric Chart of the Oceans), maps the global bathymetry with a resolution of 15 arc-seconds—were typically calculated by combining measured sea depth from echo sounding data and predicted seafloor topography information from other sources like gravity data [4–6]. However, bathymetry modeling over seamount areas is challenging due to the complex environment, such as dramatic seafloor topography drop-off and unstable current motion, as well as the scarcity of sounding data. These issues lead to the limited accuracies of current global bathymetry models over seamount regions.

The seafloor topography varies dramatically over seamounts, and seawater mass loss causes significant changes in gravity anomalies. As a result, the variation of gravity data is sensitive to the structure of seafloor topography [7–9], and the bathymetry information inversed from gravity data is an effective way for enhancing existing global models there. The global marine gravity field has been significantly improved using multi-satellite altimetry data, and the currently released gravity model maps the marine gravity field at a mean

resolution of several kilometers with an accuracy of 3–5 mGal in open seas [10]. Furthermore, the data extracted from synthetic aperture radar (SAR) altimeters have denser spatial coverage than observations derived from conventional radar altimeters, and SAR altimetry data have a higher signal-to-noise ratio and lower speckle noise [11–13]. As a result, the incorporation of SAR-based gravity data may be beneficial for bathymetry modeling.

Based on the Parker's formula [14], the frequency domain method is a widely used tool for bathymetry computation based on the linear relationship between bathymetry data and the gravity anomaly in a limited frequency band [15,16]. This method does not require any prior geophysical information, and it is numerically efficient compared to other methods like the least-squares method. The traditionally used frequency domain method, such as the S&S (Smith and Sandwell) method [17], replaces the middle-wavelength band signals of the reference model by gravity-derived bathymetry data. However, it may be difficult using this method to fully extract the useful bathymetry information in the reference model and gravity-derived bathymetry data, and consequently, this may affect the quality of the bathymetry model. To mitigate this issue, we introduce a Kalman fusing method for properly weighting and combining the reference model and gravity-derived bathymetry data.

The Kalman filter method has been used in bathymetry modeling for years. Ghorbanidehno et al. showed that the compressed state Kalman filter (CSKF) method outperformed the ensemble-based method in terms of accuracy and robustness of the solution [18]. Moreover, the studies by Breda et al. and Seoane et al. showed that the use of an adaptive Kalman filter can improve the accuracy of inversed bathymetry in comparison to the linear interpolation method [19,20]. In the previous studies, the Kalman filter algorithm was usually used to postprocess input data in bathymetry modeling, whereas the Kalman filter algorithm is used to weight and merge different bathymetry data sets in this study. To do this, the Kalman filter approach is used as a fusion algorithm for merging two or more data sets based on the error information of these data sets. The weights of different data sets are calculated from an error model based on a distance weighting method; the Kalman gain coefficients are estimated using the error information of data, and these coefficients are used for data fusion.

In this study, we investigate the performance of the Kalman fusion algorithm in seafloor topography modeling based on satellite altimetric gravity data. Moreover, the impact of using SAR-based gravity data on local seafloor topography modeling is quantified and analyzed. The structure of this study is as follows: the Kalman fusion method is briefly introduced in Section 2. The computation of the Kalman gain coefficient and the approach to estimate the error of input data sets are introduced. The study region and data sets used for local bathymetry modeling and validation are described in Section 3. Numerical experiments are presented in Section 4, and the effects introduced from SAR-based gravity data using the Kalman fusion method on seamount bathymetry inversion are quantified and evaluated. The summary and conclusion are presented in Section 5.

2. Method

Based on the S&S method, we compute the bathymetry from gravity data based on the linear relationship between bathymetry and gravity information on a limited bandwidth in the frequency domain. The details of the S&S method are seen in Smith's study [17], and the estimated bathymetry B_p at a grid node (x, y) is expressed as

$$B_p(x, y) = B_{long}(x, y) + B_{short}(x, y) + B_{inv}(x, y) \quad (1)$$

where B_{long} is the long-wavelength component derived from a reference model, B_{short} is the short-wavelength component computed from the high-pass filter of the reference model, and B_{inv} is the bathymetry information computed from band-pass-filtered gravity data [21].

In the S&S method, the gravity-derived bathymetry replaces the spectral content of the reference model on a specific limited frequency band, and long- and short-wavelength components of the reference model as well as the gravity-derived bathymetry are added

together to calculate the final bathymetry [21]. However, this may leave out useful information of the reference model, and it affects the quality of the derived bathymetry model. To mitigate this problem, we introduce a Kalman fusion method to weight and fuse the gravity-inversed bathymetry and the reference model on this frequency band. The flow chart of the application of the Kalman fusion method in bathymetry inversion is shown in Figure 1.

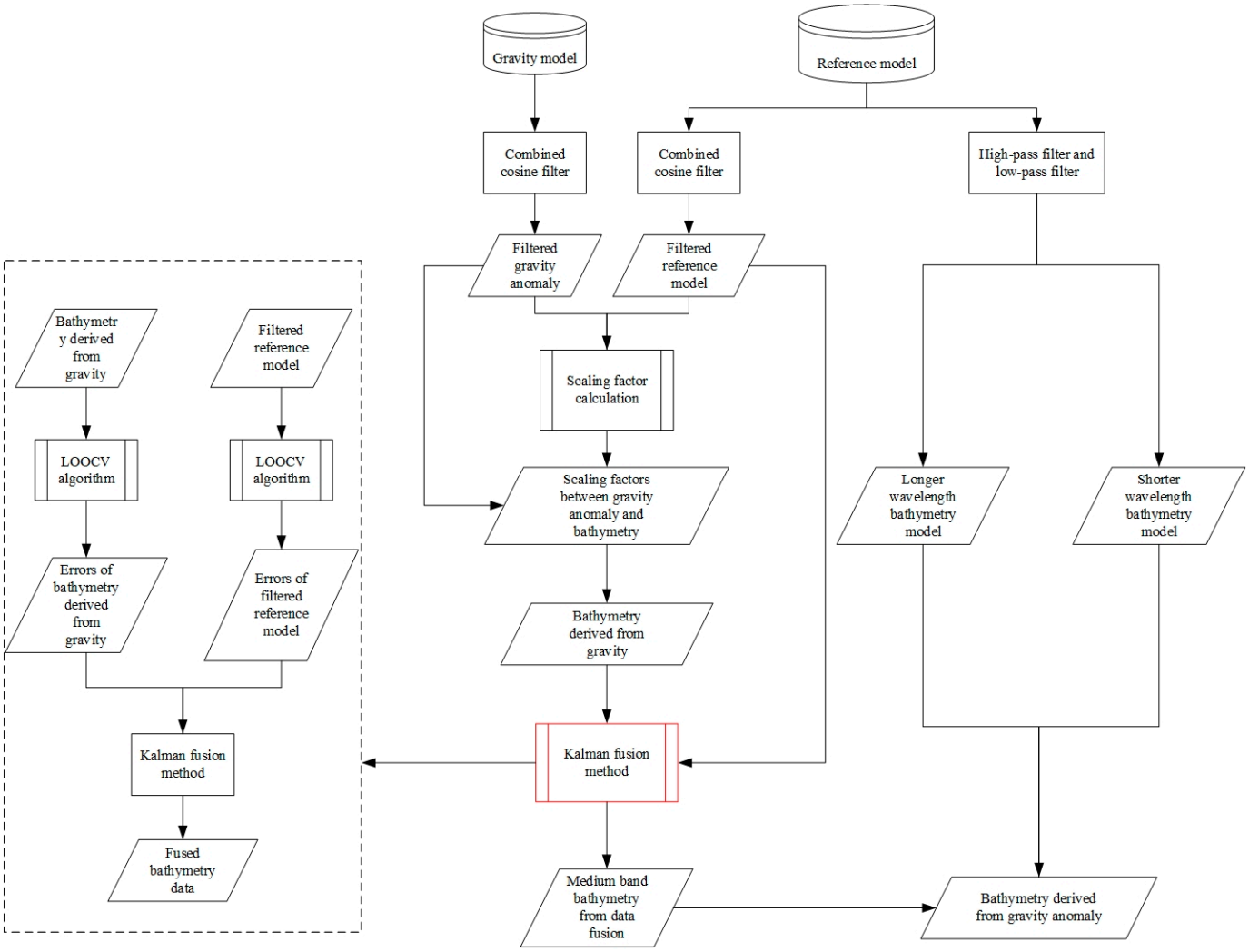

Figure 1. Flow chart of bathymetry modeling from gravity anomaly based on the Kalman filter fusion method.

2.1. Kalman Fusion Algorithm

By using the Kalman fusion algorithm, the fusion of the reference model and bathymetry derived from gravity data is expressed as

$$B_{kal}(x,y) = (I - K)B_{inv}(x,y) + K * B_{ref}(x,y) \quad (2)$$

where B_{kal} is the fused bathymetry on a limited bandwidth, B_{inv} is the bathymetry modeled from gravity data, B_{ref} is the band-pass-filtered reference bathymetry model, and K is the Kalman gain coefficient.

Once the Kalman gain coefficient has been determined, the fused bathymetry can be calculated from the reference bathymetry and gravity-derived bathymetry on a limited bandwidth. Then, the long- and short-wavelength components of bathymetry are recovered

based on Equation (1), and the final bathymetry model derived from the Kalman fusion method is

$$B_P(x,y) = B_{long}(x,y) + B_{kal}(x,y) + B_{short}(x,y) \tag{3}$$

2.2. Computation of Kalman Gain Coefficients

The key for data combination using the Kalman fusion algorithm is to determine the Kalman gain coefficient. To estimate the Kalman gain coefficient, we first construct the Kalman filter system, and the observation equation is constructed with the reference bathymetry B_0 and noise of the reference model $v(x,y)$, expressed as

$$B_{ref}(x,y) = M * B_0(x,y) + v(x,y) \tag{4}$$

where M denotes the observation matrix and (x,y) is the two-dimensional coordinate.

The inversed bathymetry is calculated from the predicted bathymetry of the previous state and the process noise $w(x,y)$, which can be expressed as

$$B_{inv}(x,y) = P * B_{kal}(x-1,y-1) + Q * w(x,y) \tag{5}$$

where (x,y) denotes the two-dimensional coordinate, P denotes the state transfer matrix, which is mainly used to transform the state optimum, and Q is the control matrix, which is used to transform the process noise variable. Here, $B_{kal}(x-1,y-1)$ denotes the predicted bathymetry of the previous state, which can be expressed as

$$B_{kal}(x,y) = B_{inv}(x-1,y-1) + K(B_{ref}(x,y) - *B_{inv}(x-1,y-1)) \tag{6}$$

where K denotes the Kalman gain coefficient.

In this study, the status observation bathymetry is composed of the inversed bathymetry derived from the gravity anomaly, and the status estimate bathymetry in the state prediction equation is based on the reference model. The state observation equation at each coordinate point can thus be expressed as

$$B_{inv}(x,y) = S(x,y) * F[g_0(x,y)] \exp[2\pi kd] W(k) \tag{7}$$

where $F[g_0(x,y)]$ denotes the filtered gravity anomaly, the parameter k is the wavenumber, and d is the depth. Here, $W(k)$ denotes the band-pass filter used in bathymetry inversion, and $S(x,y)$ shows the scale factor between the filtered reference model and the gravity value.

Based on the already-obtained status observation bathymetry $B_{inv}(x,y)$ and status estimate bathymetry $B_{ref}(x,y)$ at each coordinate point, we can calculate the predicted bathymetry $B_{kal}(x,y)$ with the Kalman gain coefficient. If the Kalman gain coefficient is set as K, the bathymetric fusion value of each coordinate point can be expressed as the proportional relationship between the inverse bathymetry and the reference bathymetry model according to the Kalman gain coefficient, which can be expressed as

$$\begin{aligned} B_{kal}(x,y) &= B_{inv}(x,y) + K(B_{ref}(x,y) - B_{inv}(x,y)) \\ &= (I-K)B_{inv}(x,y) + K * B_{ref}(x,y) \end{aligned} \tag{8}$$

In order to minimize the error in the sea depth of the coordinate point, we set the error of $B_{kal}(x,y)$ in Equation (8) to a minimum, and we obtain the Kalman gain coefficient. The error of the inversed bathymetry and the reference model will be expressed by C^{inv} and C^{ref}, respectively. The specific Kalman gain coefficient can be expressed as

$$K(x,y) = C^{inv}(x,y)[C^{inv}(x,y) + C^{ref}(x,y)]^{-1} \tag{9}$$

The Kalman fusion method used directly calculates the error of inverse bathymetry and the reference model for each point, without calculating the error of each prediction

point by iteration as in Kalman filtering. The weighting according to the directly calculated error reduces the computational complexity while ensuring the accuracy of fusion results.

2.3. Estimation of Error of Bathymetry Data

From the above study, the error of estimation bathymetry data is the key parameter for determining the Kalman gain coefficient in the Kalman fusion method. To do this, the leave-one-out-cross-validation (LOOCV) algorithm is used to calculate the error of estimation bathymetry, which is divided into a training data set and a validation data set, respectively. The training data set is used to form the training model; the validation data set is used to evaluate the accuracy of the model. Usually, the LOOCV algorithm indicates that one data set is selected as the validation data from the sample data set containing n items, and the residual $n-1$ items constitute the training sample to calculate the mean squared error (MSE). Equation (10) represents the calculation of the error of the training data set, where τ_i denotes the $i-th$ training data, and $\tau_i{}'$ denotes the prediction value of the $i-th$ training data, which is generally obtained based on the mean value or by weighting.

$$err(x,y) = \frac{1}{n-1}\sum_{i=1}^{n-1}\left(\tau_i - \tau_i{}'\right)^2 \tag{10}$$

The error of the predicted data can be obtained based on the errors of the training samples. Equation (11) represents the error calculation method for the validation data set, and (x,y) represents the corresponding points of the data.

$$E_n = \frac{1}{n-1}\sum_{k=1}^{n-1} err(x,y) \tag{11}$$

The bathymetry error of each point can be calculated based on the LOOCV method. Then, we take the bathymetry data on each point as validation data separately, with the bathymetry data around the point as the training data set, and we obtain the predicted bathymetry of validation data according to the weights of the distances. The predicted bathymetry values on the observation points can be expressed as

$$B_{Int} = \sum_{i=1}^{n} \frac{\frac{1}{t_i}}{\sum\limits_{i=1}^{n}\frac{1}{t_i}} \cdot B_i \tag{12}$$

where B_{Int} is the bathymetry of the interpolation point, B_i denotes the bathymetry of the points around the observation point, and t_i is the distance between the points around the interpolation point and the observation point. The coordinates of the points are all expressed using the WGS-84 coordinate system.

Based on Equation (12), the error of the observation point can be expressed as

$$C_{(x,y)} = B_{(x,y)} - B_{(x,y)}^{Int} \tag{13}$$

where $C_{(x,y)}$ denotes the bathymetry error at the observation point and $B_{(x,y)}$ is the bathymetry of the observation point.

The error on each coordinate point in the reference model and the inversed bathymetry data can be calculated with Equation (13), and it can be seen that the magnitude of the errors calculated with this algorithm mainly depend on the compliance between the bathymetry on each point and the interpolation result of the surrounding bathymetry data. This error calculation method can effectively reduce the signal coarseness of the input models, as well as the boundary effects generated in the signal inversion calculation. In this study, this method is mainly used to reduce the effects of the coarse difference signal in the reference bathymetry model and the boundary effect in the inversed bathymetry derived from the gravity anomaly.

3. Data and Study Area

The study area is located west of the Sjubre Bank and north of the Molloy Fracture Zone, which lies within the Arctic mid-ocean ridge system that constitutes the most active seismic source in the Arctic region. The study area extends from 79° to 80°N, and from 1° to 4°E, as shown in Figure 2a, with bathymetry data derived from the recently released global bathymetry model called GEBCO_2022 (GEBCO: General Bathymetric Chart of the Oceans) [22]. The data from the National Oceanic and Atmospheric Administration (NOAA) indicate a maximum bathymetry drop of 5153 m between the Molloy Hole and the Greenland-Spitsbergen sill. This area also contains two seamounts near the Molloy Ridge, namely, the Eistla Seamount (79.45°N, 1.945°E) and the Atla Seamount (79.36°N, 2.945°E). The Spitsbergen Fracture Zone (north of the Molloy Ridge) is a seismically active area. This study is an excellent opportunity to investigate the role of SAR altimetry data in the refinement of seafloor topography in seamount regions. It also provides fundamental data for studying the ultraslow spreading process and the thermal state of the lithosphere in the Arctic Ocean seamount region.

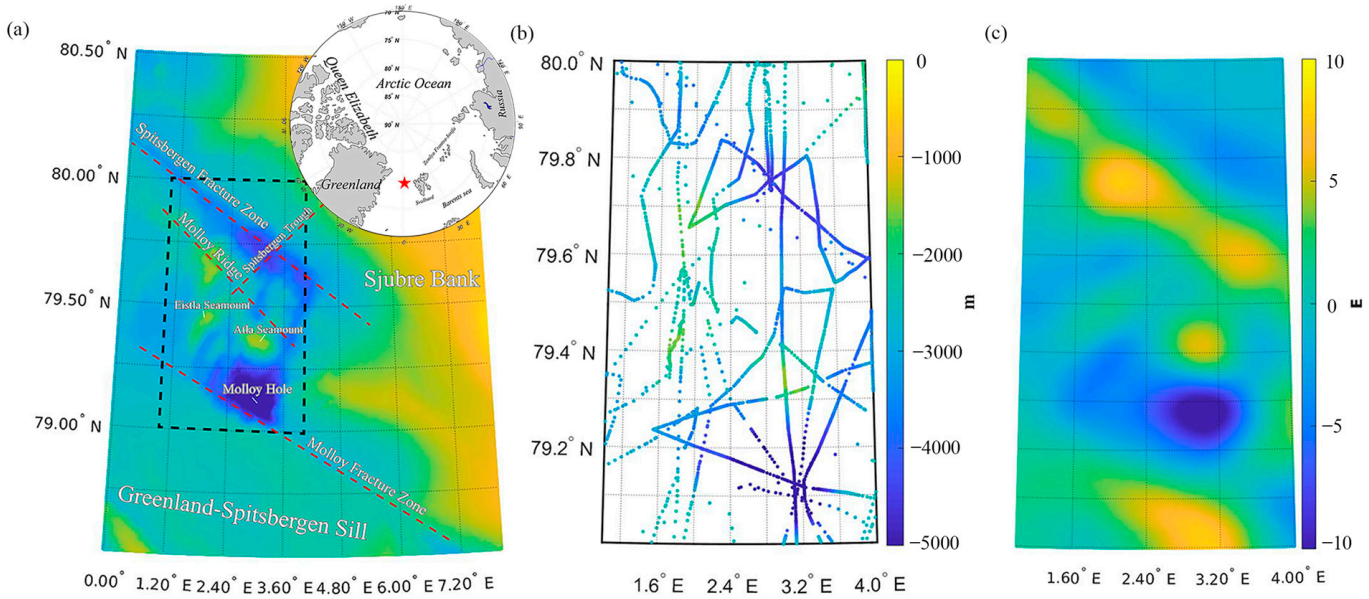

Figure 2. (**a**) Geographical overview of the Arctic Ocean where the area noted with red star is the study area. The area in the black box shows the test area. (**b**) Distribution of shipborne sounding data. (**c**) Vertical gradient of the gravity anomaly.

The local seafloor topography has strong variations: the maximum depth is 5561 m, and the shallowest depth is 1398 m, with a root mean square (RMS) of 2675.59 m. The shipborne sounding data extracted from National Centers for Environmental Information (NCEI) are sparsely distributed over the study area (see Figure 2b); however, this is a good opportunity for studying the role of altimetric gravity data in local bathymetry modeling. Moreover, the gravity information has dramatic variations over these two seamount areas; see the vertical gradient of the gravity anomaly in Figure 2c, where the vertical gradient over the Atla Seamount reaches 16.85 E (1 E = 10^{-9} s^{-2}). This offers a good opportunity to investigate the performances of using the Kalman fusion method for bathymetry modeling. The data sets used are introduced bellows.

3.1. Choice of Reference Bathymetry Model

The recently published high-resolution (15′ × 15′) global bathymetry model called GEBCO_2022 is used as the reference model in bathymetry inversion. This model used the seabed_2030 data set over the polar region, which mainly consists of shipborne sounding

data and bathymetry information predicted from satellite altimetric gravity data. Compared to its previous version, e.g., GEBCO_2014 (with a mean resolution of 30′ × 30′), GEBCO_2022 has increased its resolution to 15´. All released GEBCO models after 2019 used the Shuttle Radar Topography Mapping (SRTM) data set as the base data. Moreover, both GEBCO_2020 and GEBCO_2021 used the SRTM15+ data set as the base data in comparison to GEBCO_2019, which partly combined SRTM30+ data as the base data. Comparison with the multibeam sounding data over the southwestern part of Australia showed that SRTM15+ data have better quality than SRTM15+ V1 data, by a magnitude of 3 m. As a result, GEBCO_2022 has improved quality versus GEBCO_2021 since GEBCO_2022 uses a higher version of SRTM15+ as the base data [22,23].

3.2. Altimetric Gravity Models

To investigate the effects of SAR-based altimetric gravity data on seamount bathymetry refinement, the models released by the Technical University of Denmark (DTU) space and Scripps Institution of Oceanography (SIO) are used; see the information about these models in Table 1. For DTU models, the latest model, namely DTU21GRA, and several previous models, such as DTU17GRA and DTU15GRA, are used. Compared to DTU15GRA, the development of DTU17GRA incorporated more data from CryoSat-2 and one-year data (2016 to 2017) from SARAL/AltiKa. DTU17GRA has improved quality over DTU15GRA, where the comparison with the airborne gravity data over the northern part of Greenland showed that DTU17GRA outperforms DTU15GRA, by a magnitude of 1.67 mGal [24]. In addition, DTU21GRA included five years of Sentinel-3A and three years of Sentinel-3B and reprocessed Cryosat-2 data (processed with the SAMOSA+ physical tracker) in comparison with DTU17GRA. It is notable that CryoSat-2 operated in a low-resolution mode in the study area [25], and only DTU21GRA was calculated with SAR altimeter data from Sentinel-3A/B [26,27].

Table 1. Description of the input satellite altimeter-derived marine gravity field models.

Altimetric Gravity Model	Spatial Resolution	Year of Release	Calculated with SAR Altimeter Data?	Data Set Used in Model Development
SIO V23.1	1′	2013	No	This model was calculated by combining data from T/P, Geosat, Envisat, Jason-1, ERS-1/2, and CryoSat-2.
SIO V27.1	1′	2018	No	Introduced more data from Jason-2 and Cryosat-2.
SIO V29.1	1′	2019	Yes	Two years of data from Sentinel-3A/B were added.
SIO V30.1	1′	2020	Yes	Involved data from SARAL/Altika as well as more data from Cryosat-2 and Sentinel-3A/B.
SIO V31.1	1′	2021	Yes	Included more data from Cryosat-2, SARAL/Altika, and Sentinel-3A/B.
DTU15GRA	1′	2015	No	This model involved data from CryoSat-2 and Jason-1, and combined data from Topex/Poseidon (T/P), Geosat, ICESat, Jason-1, GFO, Envisat, and retracked data from ERS-1.
DTU17GRA	1′	2017	No	Added more CryoSat-2 data and SARAL/AltiKa data from 2016 to 2017 in the geodetic phase.
DTU21GRA	1′	2021	Yes	This model added five years of Sentinel-3A and three years of Sentinel-3B compared to DTU17GRA and calculated with reprocessed Cryosat-2 data (processed with the SAMOSA+ physical retracker).

For the models derived from SIO, the recently released model namely SIO V31.1 and several previous models like SIO V30.1, SIO V29.1, SIO V27.1, and SIO V23.1 are used [28,29]. SIO V27.1 was calculated by using more data from SARAL/AltiKa, Jason-2

and CryoSat-2 in comparison to SIO V23.1. The comparison with local gravity data in Gulf of Mexico showed that SIO V27.1 had improved accuracy over SIO V23.1, by 1.33 mGal [30]. In comparison to SIO V27.1, SIO V29.1 was computed by including three years (2017–2019) SAR altimeter data from Sentinel-3A. Moreover, the improvement of SIO V31.1 over SIO V29.1 is that the former was modeled utilizing three years (2019–2021) of Sentinel-3B data and more Sentinel-3A data.

3.3. Shipborne Sounding Data

The shipborne sounding data extracted from NCEI is used as control data to assess the computed bathymetry models. The shipborne sounding data mainly consist of single-beam and multi-beam bathymetry data, and this data set spans from 1965 to 1993 with an accuracy less than 0.5 m in deep water [31]. After excluding abnormal data, the shipborne sounding data contains a total of 2903 points, with a maximum value of 5699 m and a minimum value of 1452 m. The distribution of shipborne sounding data is shown in Figure 2b.

4. Results and Discussions

4.1. Bathymetry Calculated from Gravity Data

The computation of bathymetry from gravity data is based on the linear relationship between bathymetry and gravity information on a limited bandwidth in the frequency domain. To derive the band-pass-filtered bathymetry and gravity information, a combined cosine filter is applied to the reference bathymetry model and gravity data, respectively [21]. The maximum and minimum truncated wavelengths are selected as 130 km and 20 km, respectively; the details regarding the way we calculate the truncated wavelength are given by Wu et al. [32]. In this section, GEBCO_2022 is selected as the reference model, and SIO V31.1 is used as the input gravity anomaly. Figure 3 displays the band-limited signal within the truncated wavelength range, where Figure 3a,b show the band-pass-filtered reference model and the band-pass-filtered gravity anomaly, respectively. The bathymetry and gravity data have strong correlations, which are obvious over the two seamount and Molloy Trench areas, where seafloor topographic variations are significant.

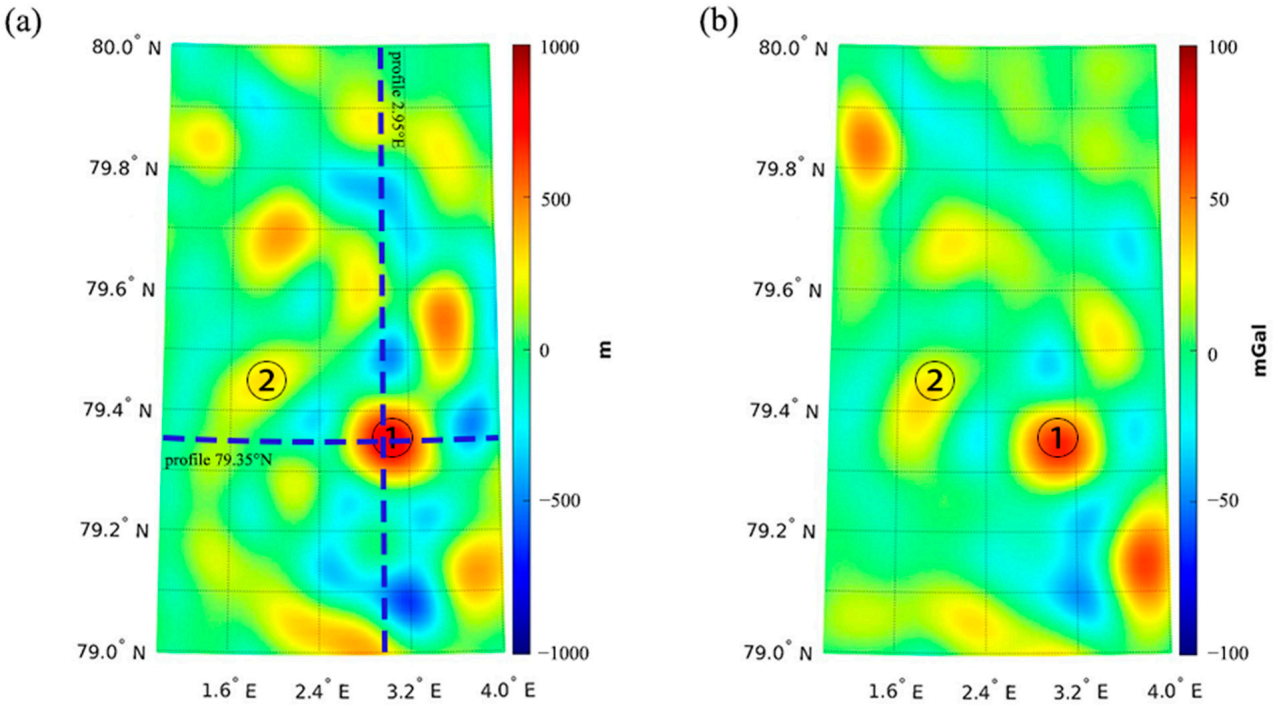

Figure 3. (**a**) Band-pass-filtered reference bathymetry and (**b**) band-pass-filtered gravity data. The dashed lines are two profiles passing through the Atla Seamount. The Atla seamount noted with area 1 and the Eistla seamount noted with area 2.

The local seafloor topography is complex, containing seamounts, oceanic ridges, sea holes, and other seafloor topography, and the computation of gravity-derived bathymetry is based on a partition method instead of selecting a sample area for scale factor calculation in the S&S method [17]. We use a partition scheme to divide the study area into several subareas for the calculation of scale factors. Moreover, the window size of the subarea is chosen as 7′ in the longitudinal direction and 14′ in the latitudinal direction. The reference model and predicted bathymetry calculated from SIO V31.1 and their misfits along the profiles (latitude 79.35°N and longitude 2.95°E) are shown in Figure 4.

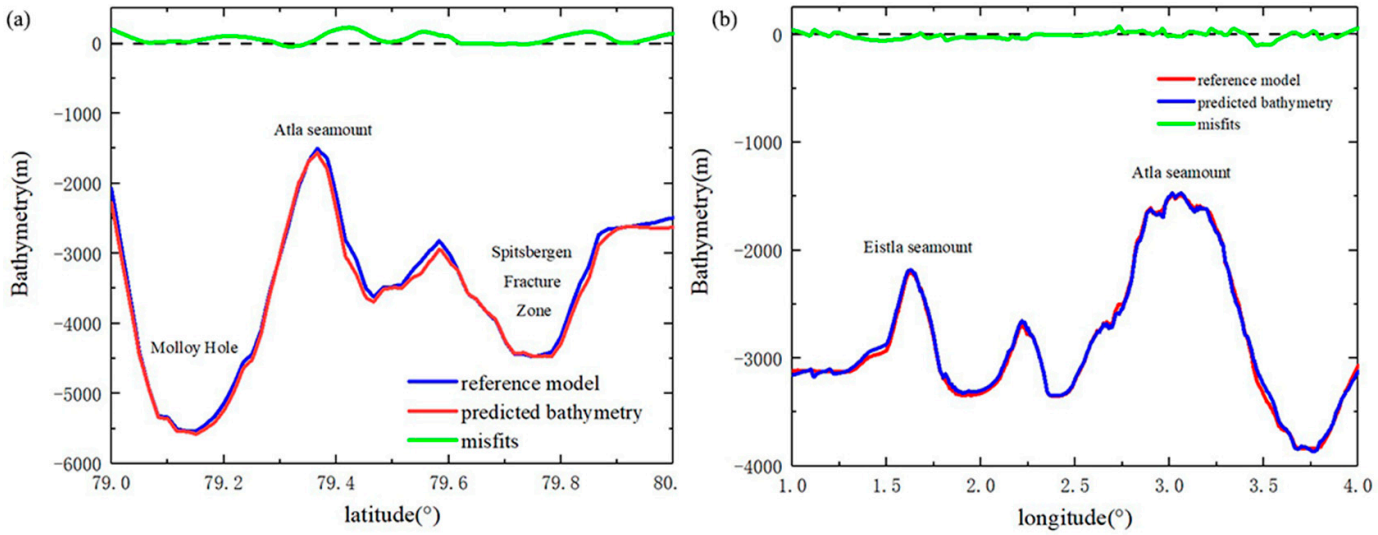

Figure 4. Difference between the filtered reference model and computed bathymetry from altimetric gravity data along profiles 2.95°E (**a**) and 79.35°N (**b**) passing through the Atla Seamount.

As seen in Figure 4, the misfits between the reference model and gravity-derived bathymetry are more prominent over seamounts and ocean hole regions than in other regions. The misfits along the profile 2.95°E (Figure 4a) are significant over the Molloy Hole (79.20°N) and Atla Seamount (79.36°N); this suggests that the bathymetry inversed from altimetric gravity data may contain additional information compared to the reference model (i.e., GEBCO_2022). Over these regions, the shipborne soundings are sparse, and the qualities of existing global bathymetry models may be limited, whereas the altimetry-derived gravity data may play a dominant role there. Thus, the improvement of altimetric gravity data by incorporating SAR altimeter data and multi-satellite altimeter data may be more pronounced in bathymetry inversion over seamounts and ocean hole regions than other regions. Moreover, the vertical gradient of the gravity anomaly over the seamount regions is stronger than that in regions with relatively flat seafloor topography (Figure 2c); consequently, the high-frequency gravity signals introduced by SAR altimetry data and radar altimeter data may be dramatic. This is possibly the reason why the misfits between the reference model and gravity-derived bathymetry are significant over these regions. We also see an observable misfit between the reference model and the gravity-derived bathymetry in the vicinity of the Eistla Seamount and Atla Seamount along latitude 79.35°N, see Figure 4b. However, the discrepancies between the reference model and gravity-derived bathymetry are significantly larger in the meridional direction (longitude 2.95°E) than in the latitudinal direction (latitude 79.35°N), which is mainly due to the variation of seafloor topography being stronger in the meridional direction than in the latitudinal direction.

4.2. Bathymetry Modeling from Kalman Fusion Method

We use the Kalman fusion method to combine the filtered reference model and gravity-derived bathymetry data. To study the influence of the Kalman fusion method, we compute local bathymetric models with the traditionally used S&S method and the updated S&S

algorithm with the Kalman fusion method, respectively. We choose the Atla Seamount and Eistla Seamount as the study areas, and the shipborne soundings within 10 km near the seamount area are used for model evaluation. We investigate the errors and weights of the reference model and gravity-derived bathymetry along two profiles (longitude 2.95°E and 1.95°E) passing through these seamount areas.

Figure 5a,b depict the errors of the reference model and bathymetry derived from the gravity model along longitude 2.95°E passing through the Atla Seamount and longitude 1.95°E through the Eistla Seamount. The predicted bathymetry error trend is similar to that of the reference model in the profile of two seamounts. The error of the predicted sea depth is generally smaller than the reference model error, by a magnitude of ~5 m in the Eistla Seamount (79.4°E). However, in some areas, the reference model errors are smaller than the predicted bathymetry errors, and we consider reducing the predicted bathymetry errors using the Kalman fusion method over these areas.

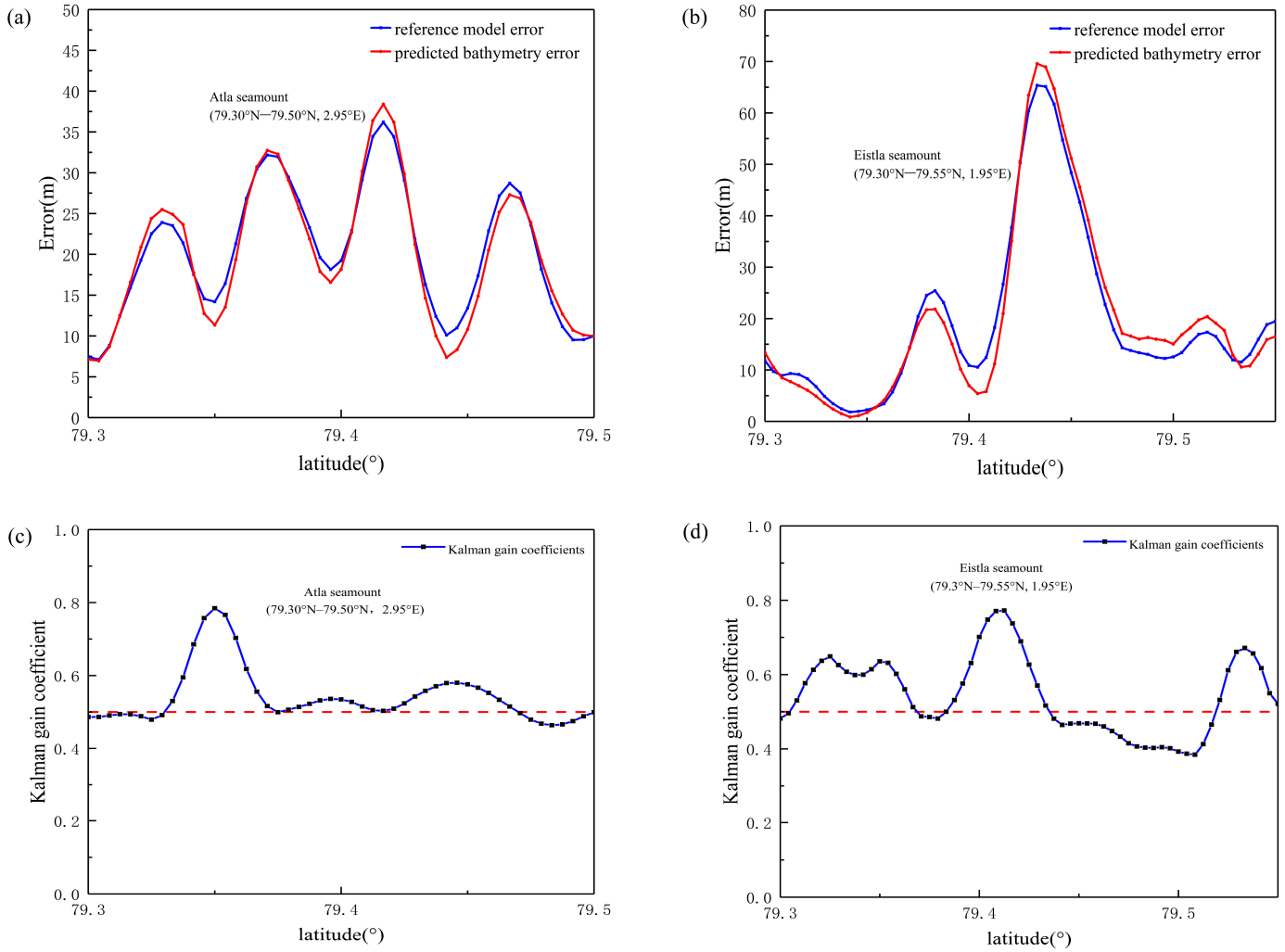

Figure 5. Error of the reference model and predicted bathymetry over (**a**) the Atla Seamount area along longitude 2.95°E and (**b**) the Eistla Seamount area along longitude 1.95°E; estimation of Kalman gain coefficients over (**c**) the Atla Seamount area along longitude 2.95°E and (**d**) the Eistla Seamount area along longitude 1.95°E.

Figure 5c,d show the Kalman gain coefficients along two profiles. A Kalman gain coefficient larger than 0.5 indicates that the fused bathymetry is more weighted by the gravity-derived bathymetry than the reference model. The Kalman gain coefficients are larger than 0.5 for most of the points along these two profiles, which reach ~0.8 for parts of the seamounts. These results indicate that the gravity-derived bathymetry may play

a more dominant role in the combined bathymetry in comparison to the reference model over seamount regions.

Moreover, the bathymetry models are computed from different approaches and validated against the sounding data over the Atla Seamount area. The model computed from the Kalman fusion method from SIO V31.1 is denoted as Model_kf_SIO31, whereas the one calculated from the S&S method is called Model_SIO31. Figure 6 shows the validation results, and the statistics are seen in Table 2. The use of the Kalman fusion method significantly improves the bathymetry modeling in comparison to the result derived from the S&S method, see Figure 6a,b. This is particularly evident along longitude 2.95°E. The statistics in Table 2 display the SD of the misfits between Model_SIO31 and shipborne soundings, which is 261.25 m, while the SD further reduces to 251.91 m when Model_kf_SIO31 is assessed. These results indicate the superiority of the Kalman fusion method versus the traditionally used S&S method since the Kalman fusion method can more reasonably weight and combine the gravity-derived bathymetry and the reference model. Moreover, for both models calculated from the S&S method and the Kalman fusion method, we find better performance than GEBCO_2022, by the magnitudes of 25.00 and 34.34 m, respectively. This suggests that the application of recently released altimetric gravity data is beneficial for enhancing existing global bathymetry models.

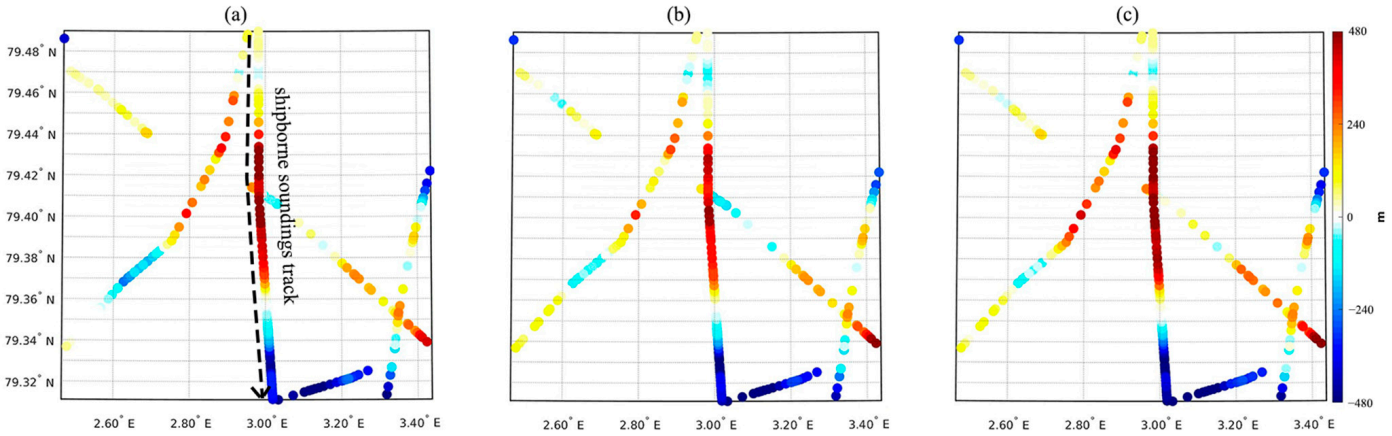

Figure 6. Differences between shipborne sounding data and (**a**) Model_SIO31 computed without the Kalman fusion method; (**b**) Model_kf_SIO31 calculated using the Kalman fusion method, and (**c**) GEBCO_2022. The dashed line represents a shipborne sounding track passing through the Atla Seamount area.

Table 2. Statistics of the misfits between different models and shipborne sounding data over the Atla Seamount area (units: m).

Model	Max	Min	Mean	SD
Model_kf_SIO31	480.99	−599.39	−10.33	251.91
Model_SIO31	542.04	−582.99	8.04	261.25
GEBCO_2022	572.72	−602.40	22.36	286.25

Local seafloor topography refinement is beneficial to the study of the interaction between the Eistla Seamount and the Spitsbergen Trough on the Molloy Ridge in regions with sparse distribution of multibeam data. It also contains fundamental data for studying the spreading motion of polar oceanic ridges.

Figure 7 shows the discrepancies between shipborne soundings and different bathymetry models along a track passing through the Atla Seamount area, and the location of this track is seen in Figure 6a. The computed bathymetry models using altimetric gravity data are better than GEBCO_2022, which are prominent near the seamount areas. By using the SAR-based altimetric gravity data, the derived bathymetry, namely Model_SIO31 using

the S&S method, is improved by 33.81 m compared to GEBCO_2022, see Table 3. The introduction of the Kalman fusion method further improves the quality of the derived bathymetry model compared to the traditionally used S&S method, by a magnitude of 76.15 m, when comparing Model_kf_SIO31 and Model_SIO31. These results also highlight the superiority of using the Kalman fusion method for bathymetry modeling. Based on these results, the Kalman fusion method instead of the S&S method is used in the following for bathymetry computation.

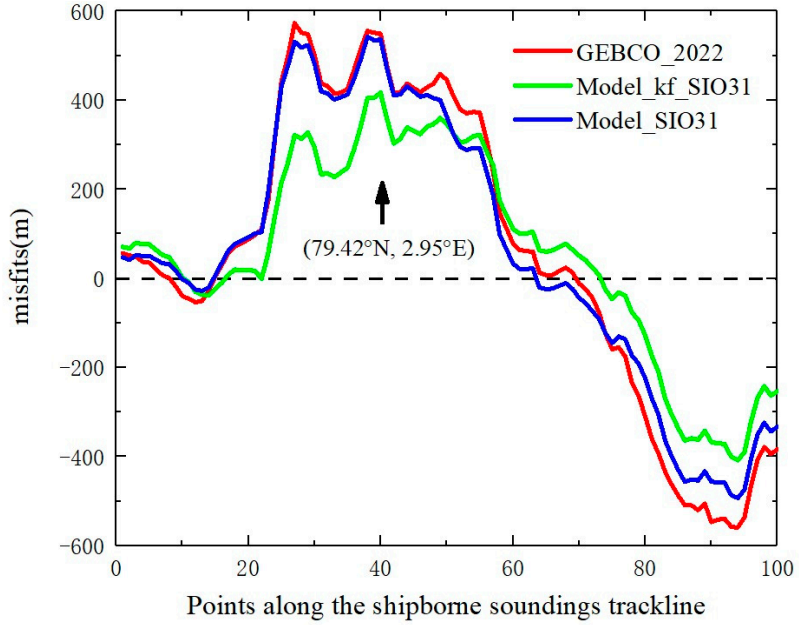

Figure 7. Discrepancies between shipborne sounding data and various bathymetry models along a shipborne sounding track over the Atla Seamount area.

Table 3. Statistics of the discrepancies between different models and shipborne sounding data along a track through the Atla Seamount area (units: m).

Model	Max	Min	Mean	SD
Model_kf_SIO31	416.72	−408.07	53.83	231.89
Model_SIO31	542.04	−493.08	55.84	308.04
GEBCO_2022	572.72	−559.24	52.75	342.32

4.3. Comparison of the Results Derived from Different Altimetric Gravity Data

In addition, we investigate the performance of different altimetry-derived gravity models in bathymetry modeling over these two seamounts. We model local seabed topography using different gravity data developed with and without SAR altimeter data since CryoSat-2 only operates with a low-resolution mode (LRM) in this region, and only SIO31, SIO30, SIO29, and DTU21GRA are the SAR-based gravity models. The shipborne sounding data within 10 km near the Atla Seamount and Eistla Seamount are used for model assessment.

4.3.1. Case Study 1: Atla Seamount

The bathymetry model derived from a specific gravity model is denoted as "Model_kf_" plus the name of this model; for instance, the bathymetry model calculated from SIO V23.1 is denoted as Model_kf_SIO23. Figure 8 shows the misfits between different bathymetry models and shipborne sounding data, and we see that the bathymetry models calculated from different altimetric gravity models have heterogeneous qualities. The statistics in Table 4 display that the SD of the misfits between shipborne sounding data and bathymetry models computed from SAR-based gravity models (i.e., Model_kf_DTU21, Model_kf_SIO31,

Model_kf_SIO30, and Model_kf_SIO29) are 254.50/251.91/253.15/253.52 m, which are reduced by 31.75/34.34/33.10/32.73 m compared to the result when GEBCO_2022 is validated. In comparison, the SD values change to 263.78/266.18/266.30/267.36 m when the bathymetry models calculated from gravity models developed without SAR altimetry data (i.e., Model_kf_DTU17, Model_kf_DTU15, Model_kf_SIO27, and Model_kf_SIO23) are validated, with a reduction of 22.47/20.07/19.95/18.89 m compared to GEBCO_2022.

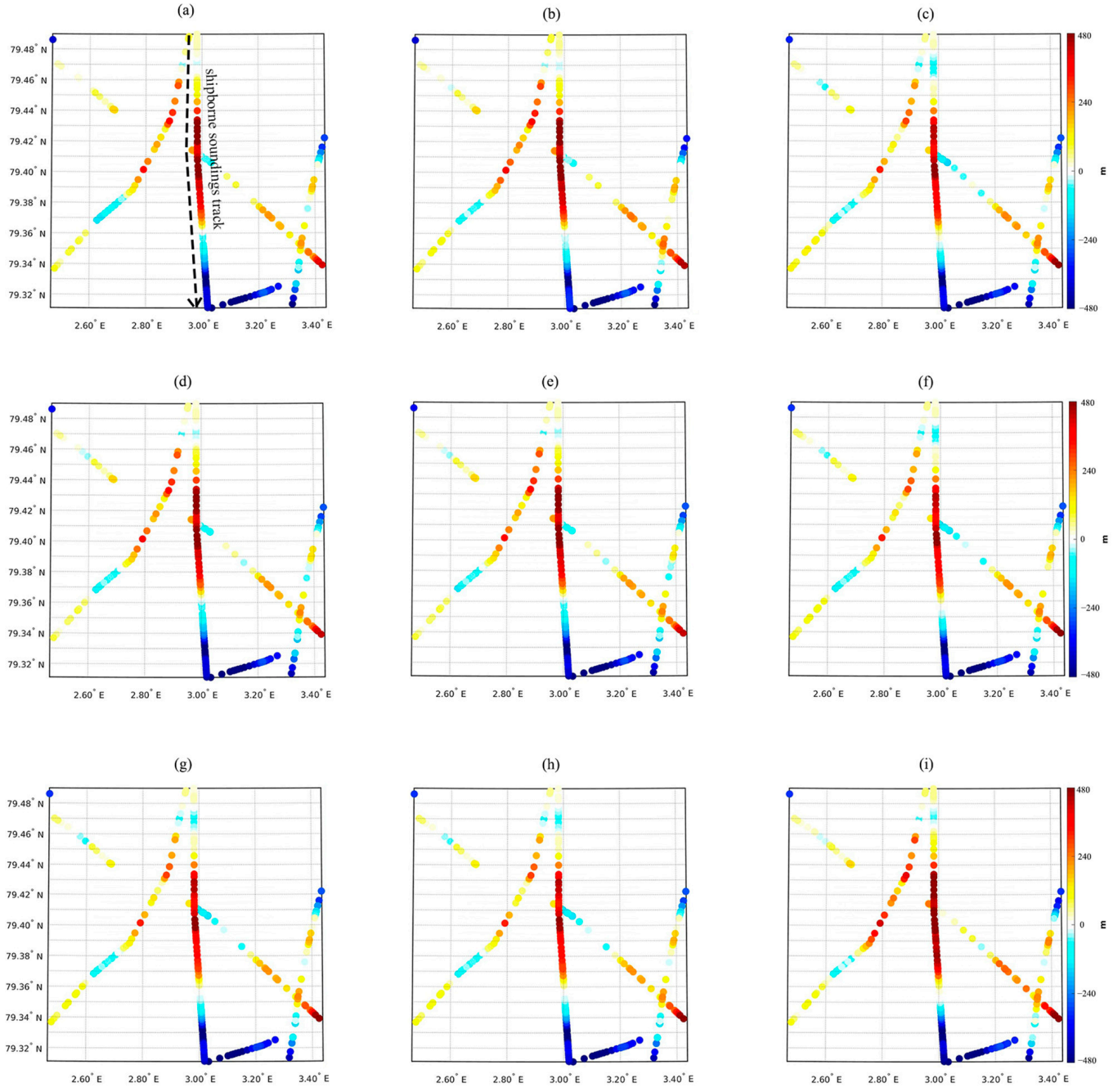

Figure 8. Misfits between the bathymetry model calculated from (**a**) DTU15GRA, (**b**) DTU17GRA, (**c**) DTU21GRA, (**d**) SIO V23.1, (**e**) SIO V27.1, (**f**) SIO V29.1, (**g**) SIO V30.1, (**h**) SIO V31.1, and shipborne sounding data over the Atla Seamount area. (**i**) demonstrates the misfits between GEBCO_2022 and shipborne sounding data. Note: only DTU21GRA, SIO V31.1, SIO V30.1, and SIO V29.1 were computed with the SAR altimetry data derived from Sentinel-3A/B over this area.

Table 4. Statistics of the differences between shipborne sounding data and different bathymetry models over the Atla Seamount area (units: m).

Model	Max	Min	Mean	SD
Model_kf_SIO23	529.15	−614.02	−2.22	267.36
Model_kf_SIO27	527.89	−613.96	−2.82	266.30
Model_kf_SIO29	482.08	−601.25	−8.72	253.52
Model_kf_SIO30	482.28	−599.65	−8.81	253.15
Model_kf_SIO31	480.99	−599.39	−10.33	251.91
Model_kf_DTU15	498.26	−617.12	−3.94	266.18
Model_kf_DTU17	519.56	−594.12	11.10	263.78
Model_kf_DTU21	487.94	−603.77	−6.55	254.50
GEBCO_2022	572.72	−602.41	22.36	286.25

The bathymetry derived from SAR-based gravity data has better performance than that derived from gravity data modeled without SAR altimetry data. For instance, the SD of the misfits is 266.30 m when Model_kf_SIO27 is assessed while the SD reduces to 251.91 m when Model_kf_SIO31 computed from the SAR-based gravity model SIO V31.1 is validated. The use SAR altimetry data developed from DTU derives similar results, where the SAR-based models derive better bathymetry information. The main reason for this is that the incorporation of the SAR altimetry data from Sentinel-3A/B improves the marine gravity field and, consequently, enhances the bathymetry modeling, especially over the seamount regions where the gravity information plays a key role.

The mutual comparisons show that Model_kf_SIO31 has better quality than Model_kf_SIO29/Model_kf_SIO30, by a magnitude of 1.61/1.24 m, although all these models are modeled with gravity data computed using SAR altimeter data. The main reason for this may be due to the fact that more observations from Cryosat-2, SARAL/Altika, and Sentinel-3A/B have been used in developing SIO V31.1, which further improves the quality of SIO V31.1 compared with SIO V29.1/SIO V30.1.

We further investigate the performance of bathymetry models along one track that passes through the Atla Seamount, and the location of this track is seen in Figure 8a. Figure 9 shows the misfits between various bathymetry models and shipborne sounding data, where two representative models computed from SAR-based gravity data (i.e., Model_kf_SIO31 and Model_kf_DTU21) and two models calculated from gravity data developed without SAR data (i.e., Model_kf_SIO27 and Model_kf_DTU17) are introduced. All four models strengthened by altimetric gravity data have better performance than GEBCO_2022. These improvements are prominent over the center of the Atla Seamount (see the arrow in Figure 9), where the bathymetry calculated with SIO V31.1 (i.e., Model_kf_SIO31) has better quality than GEBCO_2022, by a magnitude greater than 90.21 m. Moreover, the performance of bathymetry models computed with and without SAR altimetry data can also be discriminated along this track. For instance, the misfit between Model_kf_SIO31 and shipborne sounding data is reduced by approximately 60.10 m compared to the result derived from Model_kf_SIO27. However, with the increase of the distance from the seamount area to the open sea, the improvement of bathymetry modeling using SAR altimetry data gradually declines.

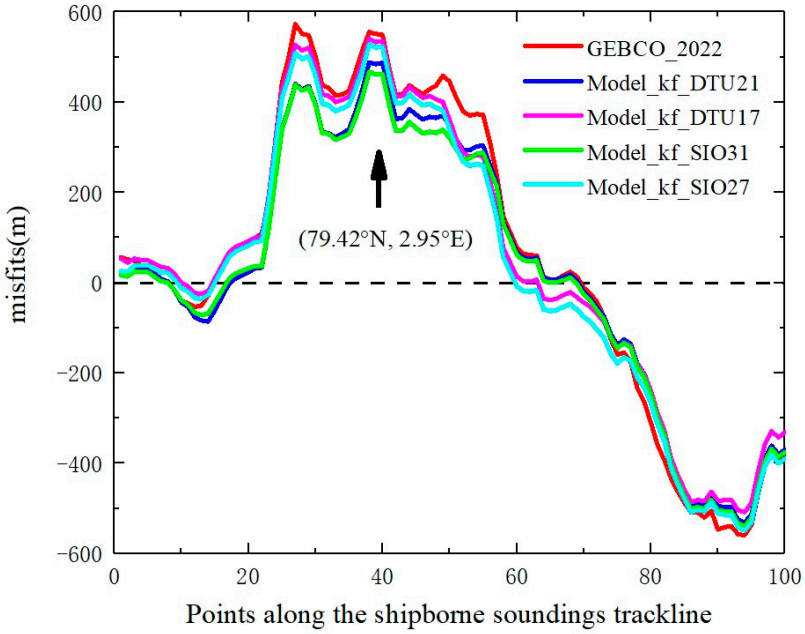

Figure 9. Misfits between shipborne sounding data and different bathymetry models along a shipborne sounding track over the Atla Seamount area.

4.3.2. Case Study 2: Eistla Seamount

In the following case, the Eistla Seamount, located west of the Molloy Ridge, is selected as the study area, and the submarine topographic variation of the Eistla Seamount is gentler than that of the Atla Seamount. Figure 10 shows the misfits between different bathymetry models and sounding data, and Table 5 provides the associated statistics. The bathymetry models enhanced by using different altimetric gravity data have a better fit with shipborne sounding data, constituting a reduction of approximately 10.43–18.49 m in terms of SD values compared to GEBCO_2022. Moreover, the validation against the sounding data can also discriminate the performances of gravity data sets computed with and without SAR altimetry data in local bathymetry modeling. For example, Model_kf_DTU21 has a better fit with sounding data than Model_kf_DTU15/Model_kf_DTU17, by a magnitude of 4.7/3.52 m. Model_kf_SIO31 and Model_kf_DTU21 have relatively high qualities among various bathymetry models, and the SD of the misfits against shipborne sounding data are 197.23 and 196.81 m, respectively.

Table 5. Statistics of the differences between shipborne sounding data and different bathymetry models over the Eistla Seamount area (units: m).

Model	Max	Min	Mean	SD
Model_kf_SIO23	532.00	−667.10	−41.30	204.87
Model_kf_SIO27	529.85	−647.67	−43.20	202.27
Model_kf_SIO29	515.97	−665.22	−44.07	198.04
Model_kf_SIO30	524.49	−655.99	−44.58	197.85
Model_kf_SIO31	519.36	−657.41	−46.88	197.23
Model_kf_DTU15	562.89	−640.18	−41.27	201.51
Model_kf_DTU17	553.17	−653.87	−39.11	200.33
Model_kf_DTU21	525.40	−659.89	−48.42	196.81
GEBCO_2022	529.40	−640.94	−20.75	215.30

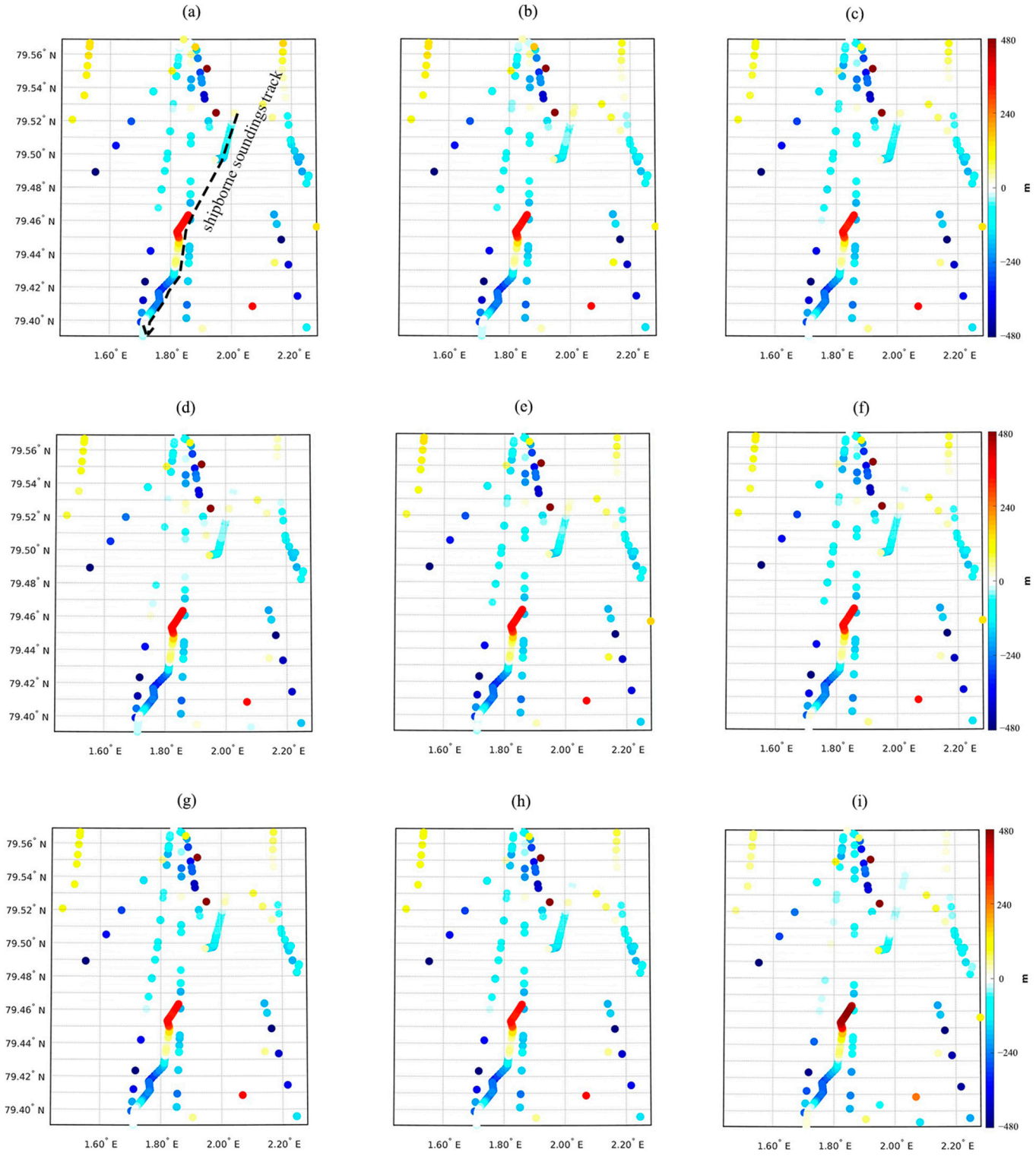

Figure 10. Misfits between the bathymetry model calculated from (**a**) DTU15GRA, (**b**) DTU17GRA, (**c**) DTU21GRA, (**d**) SIO V23.1, (**e**) SIO V27.1, (**f**) SIO V29.1, (**g**) SIO V30.1, (**h**) SIO V31.1, and shipborne sounding data over the Eistla Seamount area. (**i**) demonstrates the misfits between the GEBCO_2022 model and shipborne sounding data.

Moreover, we compare different bathymetry models and shipborne sounding data along a shipborne sounding track across this seamount, the location of which can be seen in Figure 10a. As shown in Figure 11, the performance of inversed bathymetry models calculated from altimetric gravity data is better than GEBCO_2022. For instance, Model_kf_SIO31

has improved quality versus GEBCO_2022, by a magnitude of 69.31 m over the center of the Eistla Seamount (see the arrow in Figure 11). Similarly, by introducing SAR altimetric gravity data, the derived bathymetry is improved in comparison to that derived from gravity data calculated without SAR data. This improvement reaches a magnitude of ~10.58 when we are comparing Model_kf_SIO31 and Model_kf_SIO27, for instance. However, the improvement introduced by SAR-based gravity data is not as obvious as the result derived from the case over the Atla Seamount. This may be mainly due to the relatively smooth seafloor topographic variation over the Eistla Seamount, and the contribution of SAR altimetry data may not be that prominent in bathymetry enhancement.

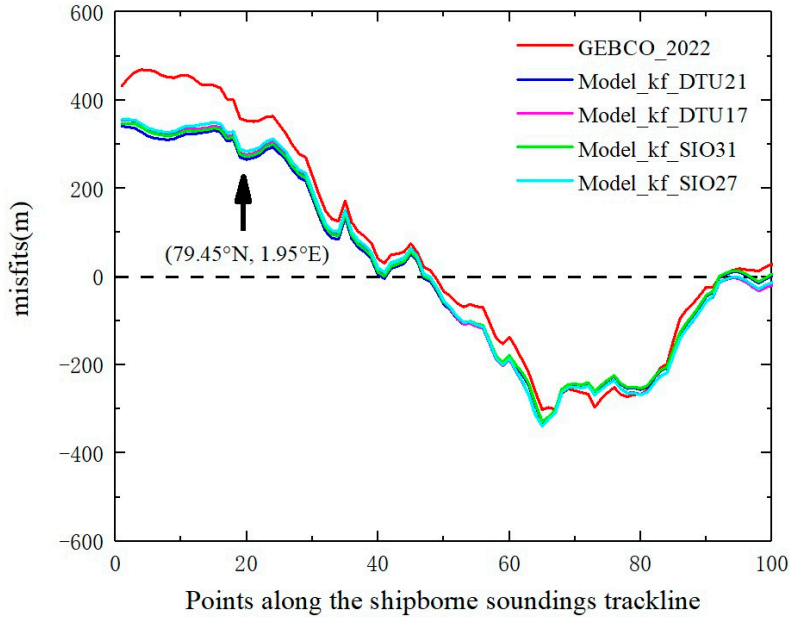

Figure 11. Misfits between shipborne sounding data and different bathymetry models along a shipborne sounding track over the Eistla Seamount area.

5. Conclusions

In this study, the satellite altimeter-derived gravity model is used to refine seafloor topography over seamount regions; in particular, we investigate the feasibility of seamount bathymetry enhancement using SAR-based gravity data. In addition, considering the difficulty for data fusion in the traditionally used filtering method, we introduce the Kalman fusion method for more reasonably weighting and combining gravity-derived bathymetry and the reference model.

Numerical results in the seamounts over the Molloy Ridge show that the incorporation of recently released altimetric gravity data improves local bathymetry inversion. The accuracy of the bathymetry modeled from gravity data computed using Sentinel-3A/B SAR altimeter data is better than that derived from the gravity data developed without SAR altimeter data, by a magnitude of 14.27 m within a 10-km area near the seamount regions.

Moreover, the proposed Kalman fusion method outperforms the traditionally used S&S method, and the bathymetry computed from the Kalman fusion method is improved by 9.34 m over the Molloy Ridge. The use of the Kalman fusion method can reasonably weight and combine the gravity-derived bathymetry and reference bathymetry model, and consequently, it can improve the bathymetry model. The application of the Kalman fusion method is not only limited in the seamount regions, but it can also be used in other areas where the altimetric gravity data play a key role in bathymetry modeling. The bathymetry model computed in this study has improved quality compared with the recently released global bathymetry model, namely GEBCO_2022, by a magnitude of 34.34 m. This indicates our solution may be substituted for existing global bathymetry models for geophysical investigations over the study area.

The bathymetric model derived from SAR altimetry data based on the Kalman fusion method can provide additional details of seafloor topography over seamount regions compared to the reference model. The refined bathymetry in this study aids in determining the boundary between the Eurasian and North American plates. Meanwhile, it provides fundamental data for lithospheric large-scale geological investigations and polar seismic studies.

Author Contributions: Conceptualization, Y.W. and J.W.; methodology, J.W. and Y.W.; software, J.W. and Y.W.; validation, Y.W. and J.W.; formal analysis, Y.W. and J.W.; investigation, Y.W. and J.W.; resources, Y.W.; data curation, J.W.; writing—original draft preparation, J.W. and Y.W.; writing—review and editing, Y.W. and Y.S.; visualization, J.W. and Y.L.; supervision, Y.W. and D.J.; project administration, Y.W.; funding acquisition, Y.W. All authors have read and agreed to the published version of the manuscript.

Funding: This study was supported by the National Natural Science Foundation of China (No. 42004008), the Natural Science Foundation of Jiangsu Province, China (No. BK20190498), the Fundamental Research Funds for the Central Universities (No. B220202055), and the State Scholarship Fund from the Chinese Scholarship Council (No. 201306270014).

Data Availability Statement: Not applicable.

Acknowledgments: The authors would like to thank the three anonymous reviewers for their constructive suggestions and comments, which were of great value for improving the manuscript. We gratefully acknowledge the funders of this study.

Conflicts of Interest: The authors declare no conflict of interest.

References

1. Leitner, A.B.; Neuheimer, A.B.; Drazen, J.C. Evidence for long-term seamount-induced chlorophyll enhancements. *Sci. Rep.* **2020**, *10*, 1–10. [CrossRef]
2. Yang, H.; Liu, Y.; Lin, J. Geometrical effects of a subducted seamount on stopping megathrust ruptures. *Geophys. Res. Lett.* **2013**, *40*, 2011–2016. [CrossRef]
3. Jiang, X.; Dong, C.; Ji, Y.; Wang, C.; Shu, Y.; Liu, L.; Ji, J. Influences of Deep-Water Seamounts on the Hydrodynamic Environment in the Northwestern Pacific Ocean. *J. Geophys. Res. Oceans* **2021**, *126*, e2021JC017396. [CrossRef]
4. Weatherall, P.; Marks, K.M.; Jakobsson, M.; Schmitt, T.; Tani, S.; Arndt, J.E.; Rovere, M.; Chayes, D.; Ferrini, V.; Wigley, R. A new digital bathymetric model of the world's oceans. *Earth Space Sci.* **2015**, *2*, 331–345. [CrossRef]
5. Ramillien, G.; Cazenave, A. Global bathymetry derived from altimeter data of the ERS-1 geodetic mission. *J. Geodyn.* **1997**, *23*, 129–149. [CrossRef]
6. Babbel, B.J.; Parrish, C.E.; Magruder, L.A. ICESat-2 Elevation Retrievals in Support of Satellite-Derived Bathymetry for Global Science Applications. *Geophys. Res. Lett.* **2021**, *48*, e2020GL090629. [CrossRef]
7. Watts, A.B.; Tozer, B.; Harper, H.; Boston, B.; Shillington, D.J.; Dunn, R. Evaluation of Shipboard and Satellite-Derived Bathymetry and Gravity Data Over Seamounts in the Northwest Pacific Ocean. *J. Geophys. Res. Solid Earth* **2020**, *125*, e2020JB020396. [CrossRef]
8. Døssing, A.; Hansen, T.; Olesen, A.; Hopper, J.; Funck, T. Gravity inversion predicts the nature of the Amundsen Basin and its continental borderlands near Greenland. *Earth Planet. Sci. Lett.* **2014**, *408*, 132–145. [CrossRef]
9. Childers, V.A.; Brozena, J.M.; Laxon, S.W.; McAdoo, D.C. New gravity data in the Arctic Ocean: Comparison of airborne and ERS gravity. *J. Geophys. Res. Solid Earth* **2001**, *106*, 8871–8886. [CrossRef]
10. Wu, Y.; Abulaitijiang, A.; Andersen, O.B.; He, X.; Luo, Z.; Wang, H. Refinement of Mean Dynamic Topography Over Island Areas Using Airborne Gravimetry and Satellite Altimetry Data in the Northwestern South China Sea. *J. Geophys. Res. Solid Earth* **2021**, *126*, e2021JB021805. [CrossRef]
11. Zhu, C.; Guo, J.; Gao, J.; Liu, X.; Hwang, C.; Yu, S.; Yuan, J.; Ji, B.; Guan, B. Marine gravity determined from multi-satellite GM/ERM altimeter data over the South China Sea: SCSGA V1.0. *J. Geodesy* **2020**, *94*, 1–16. [CrossRef]
12. Galin, N.; Wingham, D.J.; Cullen, R.; Francis, R.; Lawrence, I. Measuring the Pitch of CryoSat-2 Using the SAR Mode of the SIRAL Altimeter. *IEEE Geosci. Remote Sens. Lett.* **2014**, *11*, 1399–1403. [CrossRef]
13. Wu, Y.; Wang, J.; Abulaitijiang, A.; He, X.; Luo, Z.; Shi, H.; Wang, H.; Ding, Y. Local Enhancement of Marine Gravity Field over the Spratly Islands by Combining Satellite SAR Altimeter-Derived Gravity Data. *Remote Sens.* **2022**, *14*, 474. [CrossRef]
14. Parker, R.L. The rapid calculation of potential anomalies. *Geophys. J. R. Astron. Soc.* **1973**, *31*, 447–455. [CrossRef]
15. Hu, M.Z.; Li, J.C.; Li, H.; Shen, C.Y.; Jin, T.Y.; Xing, L.L. Predicting Global Seafloor Topography Using Multi-Source Data. *Mar. Geodesy* **2014**, *38*, 176–189. [CrossRef]
16. Li, Q.Q.; Bao, L.F. Comparative Analysis of Methods for Bathymetry Prediction from Altimeter-derived Gravity Anomalies. *Hydrogr. Surv. Charting* **2016**, *36*, 1–4.

17. Smith, W.H.F.; Sandwell, D. Bathymetric prediction from dense satellite altimetry and sparse shipboard bathymetry. *J. Geophys. Res. Solid Earth* **1994**, *99*, 21803–21824. [CrossRef]
18. Ghorbanidehno, H.; Lee, J.; Farthing, M.; Hesser, T.; Kitanidis, P.K.; Darve, E.F. Novel Data Assimilation Algorithm for Nearshore Bathymetry. *J. Atmos. Ocean. Technol.* **2019**, *36*, 699–715. [CrossRef]
19. Brêda, J.P.L.F.; Paiva, R.C.D.; Bravo, J.M.; Passaia, O.A.; Moreira, D.M. Assimilation of Satellite Altimetry Data for Effective River Bathymetry. *Water Resour. Res.* **2019**, *55*, 7441–7463. [CrossRef]
20. Seoane, L.; Ramillien, G.; Beirens, B.; Darrozes, J.; Rouxel, D.; Schmitt, T.; Salaün, C.; Frappart, F. Regional Seafloor Topography by Extended Kalman Filtering of Marine Gravity Data without Ship-Track Information. *Remote Sens.* **2021**, *14*, 169. [CrossRef]
21. Abulaitijiang, A.; Andersen, O.B.; Sandwell, D. Improved Arctic Ocean Bathymetry Derived from DTU17 Gravity Model. *Earth Space Sci.* **2019**, *6*, 1336–1347. [CrossRef]
22. Tozer, B.; Sandwell, D.T.; Smith, W.H.F.; Olson, C.; Beale, J.R.; Wessel, P. Global Bathymetry and Topography at 15 Arc Sec: SRTM15+. *Earth Space Sci.* **2019**, *6*, 1847–1864. [CrossRef]
23. Kapoor, D.C. General bathymetric chart of the oceans (GEBCO). *Mar. Geodesy* **1981**, *5*, 73–80. [CrossRef]
24. Andersen, O.B.; Knudsen, P. The DTU17 Global Marine Gravity Field: First Validation Results. In *International Association of Geodesy Symposia*; Springer: Berlin/Heidelberg, Germany, 2019.
25. Idžanović, M.; Ophaug, V.; Andersen, O.B. Coastal sea level from CryoSat-2 SARIn altimetry in Norway. *Adv. Space Res.* **2018**, *62*, 1344–1357. [CrossRef]
26. Bonnefond, P.; Laurain, O.; Exertier, P.; Boy, F.; Guinle, T.; Picot, N.; Labroue, S.; Raynal, M.; Donlon, C.; Féménias, P.; et al. Calibrating the SAR SSH of Sentinel-3A and CryoSat-2 over the Corsica Facilities. *Remote Sens.* **2018**, *10*, 92. [CrossRef]
27. Donlon, C.; Berruti, B.; Buongiorno, A.; Ferreira, M.-H.; Féménias, P.; Frerick, J.; Goryl, P.; Klein, U.; Laur, H.; Mavrocordatos, C.; et al. The Global Monitoring for Environment and Security (GMES) Sentinel-3 mission. *Remote Sens. Environ.* **2012**, *120*, 37–57. [CrossRef]
28. Sandwell, D.T.; Garcia, E.; Soofi, K.; Wessel, P.; Smith, W.H.F. Towards 1mGal global marine gravity from CryoSat-2, Envisat, and Jason-1. Lead. *Edge* **2013**, *32*, 892–899. [CrossRef]
29. Sandwell, D.T.; Müller, R.D.; Smith, W.H.F.; Garcia, E.; Francis, R. New global marine gravity model from CryoSat-2 and Jason-1 reveals buried tectonic structure. *Science* **2014**, *346*, 65–67. [CrossRef]
30. Sandwell, D.T.; Harper, H.; Tozer, B.; Smith, W.H. Gravity field recovery from geodetic altimeter missions. *Adv. Space Res.* **2019**, *68*, 1059–1072. [CrossRef]
31. Zhao, D.; Wu, Z.; Zhou, J.; Zhang, K.; Luo, X.; Wang, M.; Liu, Y.; Zhu, C. From 10 m to 11000 m, Automatic Processing Multi-Beam Bathymetric Data Based on PGO Method. *IEEE Access* **2021**, *9*, 14516–14527. [CrossRef]
32. Wu, Y.; Wang, J.; He, X.; Wu, Y.; Jia, D.; Shen, Y. Coastal bathymetry inversion using SAR-based altimetric gravity data: A case study over the South Sandwich Island. *Geodesy Geodyn.* **2022**. [CrossRef]